Structural and Spectroscopic Investigations of Bulk Poly[bis(2-ethyl)hexylfluorene]

B. Tanto,[†] S. Guha,[§] C. M. Martin,[§] U. Scherf,[‡] and M. J. Winokur*,[†]

Department of Physics, University of Wisconsin, Madison, Wisconsin 53706; Bergische Universität Wuppertal, Makromolekulare Chemie, Wuppertal, Germany; and Department of Physics, University of Missouri, Columbia, Missouri 65211

Received May 19, 2004; Revised Manuscript Received September 25, 2004

ABSTRACT: X-ray diffraction, optical spectroscopy (photoluminescence, photoluminescence excitation, Raman scattering), and molecular modeling are used in a broad study of structure and structural phase behavior within bulk poly(9,9-bis(2-ethylhexyl)fluorene-2,7-diyl) (PF2/6). The nascent polymer initially appears in a disordered state, but annealing at modest temperatures, just above the glass transition temperature (T_g) of 332 K, initiates structural evolution toward the well-known hexagonal-type phase. Cooling from the high-temperature liquid crystal mesophase yields the same basic phase structure but with much improved long-range order. Despite these large-scale changes in the PF2/6 interchain ordering, optical spectroscopy resolves only subtle variations in the spectroscopic features. Thermal cycling above 330 K (near T_g) yields red shifts in the Franck−Condon (FC) emission. These shifts are, in part, irreversible, but temperatures above 250 K retain a persistent red shift of the FC emission on heating. Temperatures above 330 K (near T_g) show little frequency shift of the Raman-active modes until cycling to temperatures above that of the liquid crystalline phase transition (at 430 K). Thereafter, monotonic shifts are observed. Excitation measurements clearly resolve two distinct defect emission peaks and specify a mobility edge for singlet exciton migration at reduced temperatures. Structure factor refinements are consistent with a 5/2 polyfluorene helix incorporating a multitude of structurally distinct conformational isomers. The alkyl side chains include conformational disorder as well and are oriented, on average, perpendicular to the helices. Combinatorial modeling of over 4000 structural isomers (i.e., gas-phase decamers at zero temperature) identifies a relatively large number of energetically favorable chain conformations. Models approximating 5/1 and 5/2 helices yield stable, low-energy structures. Preference for a 5/2 helix cannot be rigorously established at present.

I. Introduction

Polyfluorenes (PFs) are prime examples of π-conjugated polymers having optical emission peaked in the blue, good quantum efficiencies and excellent prospects for device applications.[1−3] To tailor the explicit molecular level properties, almost all PF derivatives utilize solubilizing side chain substituents anchored at the bridging carbon atom. This carbon bridge atom provides two substitution sites and also acts to coplanarize pairs of adjacent phenylene rings. Side chain substitution, in addition to simply improving the solution processing and film forming characteristics, is used to confer new functionality and alter the intramolecular and intermolecular structure at nanometer length scales.[4−6]

Much current research is directed at understanding the relationships between the side chain moiety and the observed physical properties.[7] At the simplest level bulky side chain constituents will reduce close packing of the conjugated polymer backbones[8] and thereby diminish the formation of interchain electronic pathways and optical excitations (e.g., excimers, exciplexes, etc.). These side chains can also give rise to a rich array of mesomorphic behavior with the appearance of liquid crystal polymer (LCP) phases.[9−11] Use of side chains containing chiral centers creates opportunities for optical activity and the emission of circularly polarized light.[12,13]

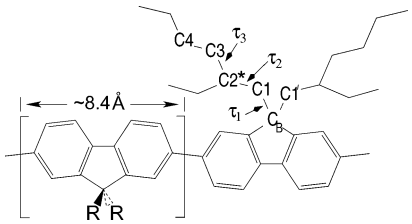

Figure 1. Sketch of the PF2/6 structure depicting CC dihedral angles of interest.

There is a pronounced sensitivity of these attributes to even slight changes in the side chain length and branching. Three closely related PF derivatives, poly(di-*n*-hexylfluorene) (PF6), poly(di-*n*-octylfluorene) (PF8), and poly[bis(2-ethyl)hexylfluorene] (PF2/6), have been heavily studied, and each has distinctive optical properties and phase behavior that are both polymer and sample history specific. In general, there are thermotropic mesophases and, especially in the cases of PF6 and PF8, a marked thermochromism with clear signatures of two or more distinct backbone conformations.[7,14−16] Of these three polymers, PF2/6 is perhaps most unusual for its peculiar structural properties, i.e., evidence for either a 5/1 or 5/2 helix, and the opportunities for imparting optical activity. Substitution of the ethyl group at the second carbon position of the hexyl side chain is, by construction, a chiral center (see Figure 1).

Most published PF2/6 research pertains to polymers that are racemic. These are materials containing equal proportions of the two possible enantiomers (conventionally referred to as S and R) to give a mixture of four

[†] University of Wisconsin.
[‡] Bergische Universität Wuppertal.
[§] University of Missouri.
* Corresponding author. E-mail: mwinokur@wisc.edu.

10.1021/ma049006p CCC: $27.50
Published on Web 11/18/2004

distinct fluorene isomers (SS, SR, RS, and RR). Despite this molecular level disorder, thermally annealed PF2/6 films exhibit an ordered hexagonal-type phase having coherence lengths exceeding 50 nm and a unit cell which incorporates three polymer chains. Oriented fiber and film studies by Lieser et al.[17] have identified X-ray and electron scattering features most consistent with a 5/2 or, less likely, a 5/1 helix of the skeletal backbone. Quantum chemical calculations of model oligomers indicate that a 5/2 helix agrees best with the experimentally observed $\pi-\pi^*$ interband transition energy.[17]

Numerous issues concerning the nature of the local chain structure, side chain organization, and interchain packing remain poorly understood. Most models presented so far generally pertain to single polymer chains in an idealized setting.[17,18] In linearly unsubstituted PFs, specifically PF8 and PF6, one possible picture is that the side chains tend toward an all-anti conformation, and these side chains are oriented nearly perpendicular to the fluorene backbone.[7] Di-*n*-octylfluorene monomers form single crystals, and crystallographic studies of these clearly identify this type of side chain behavior.[19] This characteristic may not extend to all PF polymers although recently Chen et al.[20] report good agreement with equatorial scattering data by using this side conformation as a starting point. Other modeling studies of the polymer indicate that side chains with gauche-type conformers have energies comparable to the all-anti case and, in the absence of interchain interactions, can adopt backbone torsion angle with large deviations from planarity.[18] Few reported 3D models incorporate both of these attributes.[21−23]

For PF2/6 the situation is in a similar state of affairs. The addition of the ethyl branch alters the local anti/gauche energy scales of the hexyl chain so that a more twisted side chain conformation is adopted.[17] Recent modeling studies in work by Knaapila et al.[22] can physically pack three PF chains together into a complex 5-fold helix consisting of, on average, repeating fluorene *cisoid*−*transoid* dyad pairs. Also appearing in this work is an electron density map from X-ray grazing incidence thin film data, and this analysis substantiates a three-chain construction within the PF2/6 unit cell of the ordered phase. Molecular dynamics calculations of chiral substituted fluorene oligomers containing a single enantiomer identify a strong molecular level tendency toward a helical construction.[13] As yet there is little understanding of the molecular level origins of the five monomer helix repeat in PF2/6 and the extent of conformational disorder that is present along the polymer backbone. In addition, there is almost no information available concerning the allowed side chain conformations and how these chains pack into a 3D ordered structure. Finally, there are few studies that closely cross-correlate structural evolution on thermal cycling with changes in the optical properties.

This work presents a broad study of PF2/6 bulk materials as they progress toward the ordered hexagonal phase during thermal cycling. The results for PF2/6 strongly contrast with those for PF8 and PF6 because the latter polymers often exhibit a close correlation between structural phase behavior and the optical properties. In PF2/6 the impact from large-scale structural evolution is, at first glance, far subtler. In the work that follows powder X-ray diffraction (XRD) results are reported first, and these readily identify the systematic variations in the average intrachain and interchain structures. Photoluminescence (PL)/photoluminescence excitation (PLE) spectra appear second, and this assesses the impact of thermotropic phase behavior on the optical properties of the conjugated backbone. Macro-Raman scattering is next and, in the wavenumber range scanned, primarily resolves the local vibronic characteristics of the polyfluorene backbone. Modeling calculations are presented last. At first we introduce a specific starting chain conformation in conjunction with a restricted linked-atom least-squares structure factor refinement to give a physically viable 3D model for PF2/6. Then a more exhaustive search for low-energy single chain conformations is conducted (at zero temperature and in the gas phase). These latter two topics provide a limited insight into the underlying reasons for the appearance of helices, the extent of chain conformational disorder, and the nature of the ordered state.

II. Experimental Procedure

PF2/6 samples studied were prepared using standard procedures reported previously.[1,24] The polymers were synthesized by the so-called Yamamoto procedure (with $Ni(COD)_2$ as reagent) starting from the corresponding dibromofluorene monomer. PF2/6 was precipitated from toluene into methanol, followed by a careful Soxhlet extraction with ethyl acetate to remove low molecular weight oligomers and polymers (cutoff ca. 5000). Polymer chain characteristics, M_n 83 000 and M_w 162 000, were measuring by GPC against a polystyrene standard. The coarse fibrous aggregates were mechanically cut into smaller pieces by using a scalpel and then mounted in various sample holders. Depending on the forming conditions, PF2/6 may be glassy or semicrystalline at room temperature (rt), with a nominal glass transition temperature (T_g) for the amorphous component, as ascertained by differential scanning calorimetry at 80 °C, a crystalline to nematic LCP transition just above 165 °C and the reverse transition on cooling at ca. 132 °C. There is considerable time- and temperature-dependent hysteresis on cooling.

All X-ray diffraction experiments employed an Inel CPS-120 detector based powder diffractometer in combination with a rotating anode generator (Cu target $\lambda_{K\alpha} = 1.542$ Å). The incident monochromator consisted of an elastically bent LiF crystal monochromator and He gas-filled beam paths (to minimize absorption and air scatter). Useful scattering data were obtained in the 2θ range of 1.5°−35°. Minimum scan times were on the order of a few minutes, but the powder data shown typically represent 30−90 min data acquisition times. For this technique a ca. 0.4 mm thick slab of the PF2/6 was wedged into an aluminum support frame and placed into thermoelectrically temperature controlled stage (−25 to 180 °C).

The PL/PLE studies employed a spectrometer consisting of a 150 W Xe arc lamp (Oriel 68805) in combination with a primary monochromator (JY HT-20) and a diode array equipped analyzer monochromator (Ocean Optics USB-2000). All spectra have been corrected for both the Xe lamp spectral variations and the analyzer spectrometer spectral response (using a laboratory tungsten lamp calibrated against a NIST traceable lamp). Monochromatic light (full width at half-maximum ca. 3 nm) was focused down to an incident spot, approximately $150 \times 500\ \mu m^2$, onto a optically dense piece of the PF2/6. This, in turn, was affixed to a sapphire substrate and then mounted into a vacuum oven/cryostat optical assembly (80−530 K). Photoluminescence was collected at a 45° angle from the incident light.

The Raman spectra were measured from a piece of the PF2/6 sample affixed to the copper tail piece of a closed cycle helium refrigerator/heater (11−450 K). The Raman measurements were performed using a Spex triplemate spectrometer and the 647.1 nm line of a Kr^+ laser with 10 mW incident power in a backscattering configuration. The scattered light was detected using a cryogenically cooled CCD array detector and a holo-

graphic super-notch filter to block the elastically scattered light.

To attempt a structure refinement to the powder diffraction data, a number of trial conformers were constructed with the goal of identifying viable PF2/6 chains having a simple 5/2 helix construction and, additionally, that would also nest three-dimensionally. For simplicity, only R-type chiral side chains were considered. Most of the trial starting conformations proved difficult (if not impossible) to pack into a 3D unit cell without unphysical hard-core overlaps. In only a very few cases could a sufficiently compact side chain construction be invoked that would pack into a 3D model. These models could then be tested through subsequent Rietveld refinements assuming a five monomer repeat sequence and a nominal 40 Å chain repeat.

Comparisons to the X-ray scattering data employed structural modeling software based on a custom configured link-atom least-squares (LALS) Rietveld refinement scheme as discussed in refs 25 and 26. The LALS algorithm included hard-core packing repulsion between nonbonded C atoms. These typically constrained the nearest-neighbor distance of the carbon atoms to physically accessible values. Additional intramolecular constraints were applied to the alkyl side chain dihedral angles through a simple cosine function. All bond distances and angles were typically fixed to conventional values. The primary motivation was to provide fast computational cycle times while effectively constraining the parameter space searches and *not* to accurately reflect actual chain energetics. Because Bragg scattering reflects the average structure and does not truly assess short-range-order in systems with a high degree of local disorder, this approach may be of limited utility. The 5-fold symmetry of the PF2/6 helix is necessarily incompatible with the long-range order of the proposed hexagonal unit cell, but pentagons can pack into a hexagonal lattice with a large periodicity.[27]

By alternatively increasing and decreasing the relative contribution of the packing constraints during the Rietveld refinement trapping in local minimum was often circumvented. Analogous procedures have proven helpful in studies of other polymers.[28] Because of software limitations, all three chains comprising the hexagonal unit cell were conformationally identical, but each could be independently translated and/or rotated about the helix axis. (This unit cell is already very large.) This constraint had some virtue in that it did limit the number of free parameters that could be independently adjusted and refined. A slowly varying background profile was also required, and this reflects the presence of residual air scatter, trapped disorder, amorphous/disordered phase fractions, and other artifacts. All carbons and most hydrogens were explicitly included in the structure factor calculations.

Single chain gas-phase oligomer calculations were also conducted using empirical MM3*[29] force fields as provided in the software packages Maestro and Macromodel. Rasmol[30] software was used for visual rendering of the resulting structures. The MM3* force field has merit for comparing relative energies of various hydrocarbon conformations and packings. There is also some account of energies associated with the conjugated π bonds. All MM3* calculations employed 10 monomer long oligomers without any explicit cutoff distances. Relative energies are presented on a per monomer basis and referenced to that of the lowest energy 5/2 helix conformer (retaining backbone torsional constraints). In this study the starting backbone configuration was initially configured to give either perfect ±5/2, ±5/1, or 2/1 helices consisting of a uniform repeating monomer or, in one instance, dimers (i.e., the 2/1 helix). Because side chain conformations other than all-anti are expected, the three core side chain C−C dihedral angles (τ_1, τ_2, and τ_3 as shown in Figure 1) were initially set to one of the three well-known low-energy hydrocarbon conformations (i.e., anti, gauche, and gauche′). Thus, for each helix type there were 729 (3^6) starting conformers. Every starting model was allowed to adopt its lowest energy conformation through a two-step minimization. Initially torsional constraints were placed on the main chain dihedral angles and those of the three core C−C side chains. Thereafter, all constraints were eliminated, and the oligomer was allowed to relax until the specific energy convergence criteria were met.[31] More explicit modeling details are specified in the text. Universal efficacy of this approach is not proven, but it has been shown to be useful for identifying viable low-energy conformers in selected σ-conjugated polysilanes[21,32] and conventional polyesters.[33] At present only a single RR enantiomer was modeled (for comparisons with the RR structure adopted in the structure factor calculations), and over 4000 starting conformers were examined.

III. Results

A. X-ray Powder Diffraction. A modest number of X-ray and electron diffraction studies[17,22,34,35] of PF2/6 are published, and these primarily have examined the ordered hexagonal phase after high-temperature annealing of thin film samples. Complementing this work are in situ Raman scattering studies of films on thermal cycling[36] and differential scanning calorimetry (DSC) measurements.[37] DSC measurements typically resolve a small endotherm near 160 °C on heating, and this corresponds to the transition to a LCP phase. There is strong hysteresis on cooling. Raman scattering[38] (in PF6 and PF8) can resolve additional discrete features (many of these are of unknown origin) on thermal cycling at temperatures below the LCP transition temperature. Recent dielectric spectroscopy measurements resolve both α- and β-type relaxation processes and, of special importance here, extrapolates a glass transition temperature $T_g = 332$ K (59 °C) for an infinite chain.[39]

Of the techniques employed in this study, XRD is most able to document overt changes of the PF2/6 structure in response to thermal cycling and annealing. Characteristic XRD data are shown in Figures 2 and 3 during the first heating and cooling cycle, respectively. Most apparent are the irreversible changes in the diffraction profiles on thermal cycling. This characteristic is common to polymers and demonstrates that the as-formed bulk PF2/6 sample exists in a metastable or kinetically limited state.

These curves also resolve a number of salient characteristics. Initially (at −28 °C) this PF2/6 sample exhibits three broad scattering features centered near 2θ angles of 6.2°, 11°, and 21°. The first two occur at positions corresponding to the (100) and (110) reflection of the hexagonal phase and are indicative of an interchain packing that is qualitatively similar despite the high degree of interchain disorder. The broad 21° peak is a feature common to many side chain substituted polymers and is usually attributed to residual disorder in the packing of the alkyl side chains. The most unusual feature is a relatively sharp and asymmetric peak centered near 11.1°. This corresponds to a d-spacing of ca. 8 Å and closely matches the monomer spacing along the chain axis.

Additional evidence can be found in support of the assertion that the initial interchain packing approximates that of the more ordered hexagonal phase. We find that even modest heating above room temperature initiates a structural evolution dominated by the appearance of scattering features having peak positions characteristic of the ordered phase. Although the kinetics are very sluggish at 50 °C, an extended 12 h isothermal anneal, as indicated by comparing the respective spectra in Figure 2, produces a very slight increase in the intensities of the peaks at lower 2θ angles. Heating to 76 °C dramatically raises both the

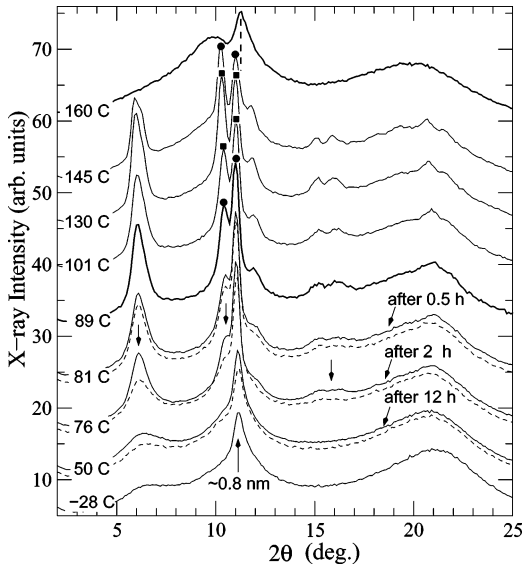

Figure 2. Powder XRD spectra from nascent PF2/6 bulk sample on heating during the first thermal cycle. Dotted lines are spectra taken during the first 30 min at the indicated soak temperatures. Symbols (filled circles and squares) are used to specify the relative maximum intensities of the equatorial (110, on left) and nonequatorial ($l = 5$ layer line, on right) scattering peaks. All spectra are offset for clarity.

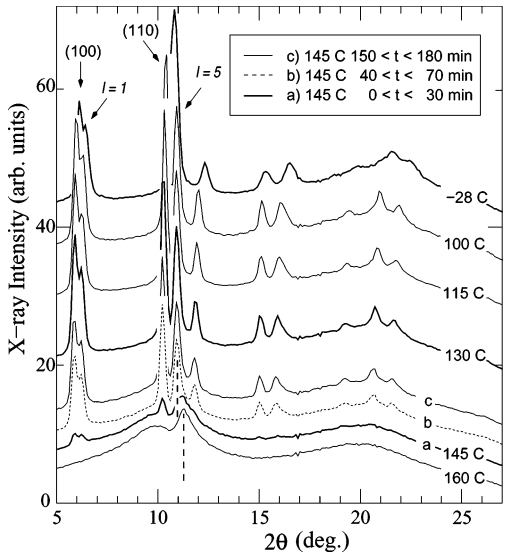

Figure 3. Powder XRD spectra from PF2/6 bulk sample on cooling during the first thermal cycle. Curves labeled a−c are from an isothermal anneal. All spectra are offset for clarity.

magnitude and rate of this change although the kinetics remain slow. All of the aforementioned peaks both sharpen and intensify, and centered about a 2θ angle of 16°, at least two new peaks can be discerned. By 81 °C we can no longer easily resolve changes in sequential spectra taken every 30 min. The onset of this interchain ordering occurs at temperatures close to that of the reported T_g and are suggestive of a cold crystallization with a broadly defined onset.

The changes seen on heating from 90 to 140 °C are modest and, given the behavior seen below 90 °C, not unexpected. Most of the hexagonal phase peaks continue to narrow and, at the lower temperatures, intensify. Up to four additional peaks appear, and these are superimposed on the broad 21° scattering peak. The 8 Å chain axis repeat peak near $2\theta = 11°$ is the only exception, and it smoothly diminishes in intensity. This suggests a molecular level competition between interchain and intrachain ordering with the former occurring at the expense of the latter. These trends become reversed in the LCP mesophase, and the peak corresponding to an 8 Å repeat is retained. This scattering sits atop the tailing edge of a broad peak centered near 11°. All features at lower 2θ angle become broadened. This is interpreted as evidence of a more uniform packing of the individual polymer chains and obscures the 3-fold packing of chains within the unit cell of the ordered hexagonal phase.

The data on cooling, as shown in Figure 3, also reveal interesting characteristics. The three sequential 145 °C spectra clearly demonstrate that the order−disorder transition to the hexagonal phase is slow. Also, discernible is an abrupt change in the *c*-axis repeat after formation of the hexagonal phase from 7.8 to 8.0 Å. The reverse process can be seen in Figure 2 on heating as well (as indicated by the dashed vertical lines). The angular 2θ widths of the various Bragg peaks are noticeably sharper than those seen on heating and, correspondingly, indicate larger coherence lengths (of ca. 50 nm). Comparable values are reported in ref 17 (PF2/6) and ref 7 (PF8). The majority of the reflections are equatorial but the $l = 1$ and 5 layer lines are both resolved, and they are explicitly identified in Figure 3.

There are a few additional attributes of note. First there is a relative increase in the height of $l = 1$ and $l = 5$ scattering at reduced temperatures. This effect arises because of a pronounced, order-dependent broadening of the equatorial peaks.[40] Freezing of the alkyl side chains and the development of large-scale strains are a likely cause.[41] This further supports the claim of molecular level competitions between intrachain and interchain ordering. There is also a pronounced anisotropy in the thermal expansion coefficients so that, at −28 °C, the (110) reflection becomes nearly superimposed on the $l = 5$ layer line scattering.

B. Photoluminescence and Photoluminescence Excitation. Extensive steady-state and time-dependent optical properties of PF2/6 are reported[42−46] in the literature. The majority of this work involves either solutions or drop-cast/spin-cast thin films. The largest contribution to either the optical absorption or emission is from an intrachain $\pi-\pi^*$ transition of approximately 2.95 eV. A well-resolved Franck−Condon (FC)-type progression of vibronic subbands is seen in addition to the main $\pi-\pi^*$ electronic transition. These vibronic bands are dominated by modes representing local C−C stretching in the vicinity of 1200−1600 cm^{-1} (or 150−200 meV). Many samples also exhibit an additional and very broad emission peak[24,47−49] that is centered near 2.5 eV. For PF2/6 the majority of this emission is thought to originate at a small number of chemical defect sites (e.g., keto type). These defects are likely to be synthesis related.[50] These sites function as local traps for migrating excitons and strongly reduce the FC emission even at low concentrations. This attribute strongly contrasts with that seen in PF6 and PF8 samples which, depending on the sample history, can have appreciable aggregate-type emission, and these are often attributed to interchain excitations.[16,51,52]

The bulk nature of these PF2/6 samples precluded use of simple photoabsorption and photoluminescence methods. For these measurements the excitation source was typically swept in 4 nm steps from 350 to 580 nm. An important consideration in this study was to perform

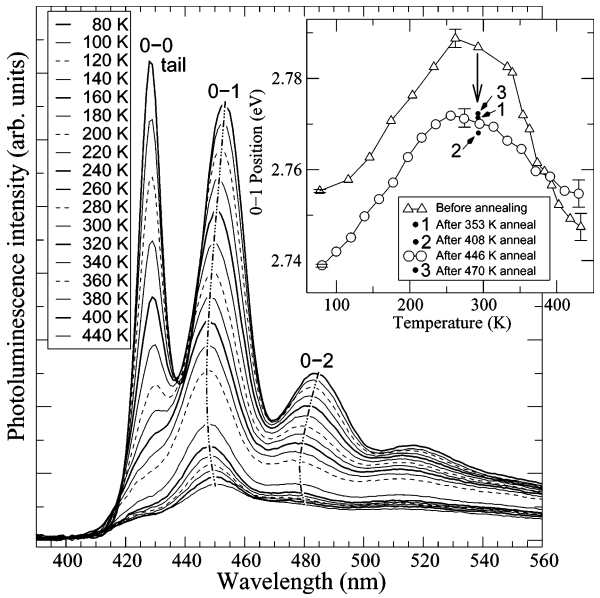

Figure 4. PL from PF2/6 bulk surface (on warming) after annealing at 446 K followed by slow cooling. Data are corrected for spectrometer response, and the excitation wavelength is 380 nm. Inset: center position of the 0−1 vibronic band during first thermal cycle (open triangles) and after multiple thermal cycles to increasingly higher temperatures (open circles).

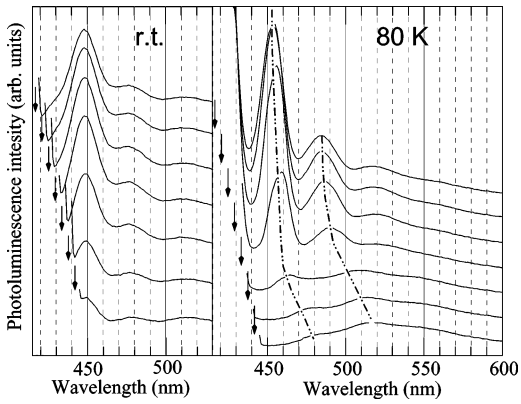

Figure 5. Example "site-selective" PL spectra of PF2/6 bulk sample at rt (on left) and at 80 K (on right) before thermal cycling/annealing. Data are offset for clarity. Vertical arrows point to the excitation wavelengths (in 4 nm steps). The two dash−dotted lines are used to visualize the mobility edge at which the vibronic band positions become strongly temperature sensitive.

optical studies using samples with comparable thermal histories in all experimental techniques. Because reduced temperatures often yield better optical spectra, the first heating cycle was executed in a stepwise fashion whereby the PF2/6 would be intermittently cooled to 80 K and the temperature-dependent PL/PLE data recorded. Figure 4 shows just one series of PL spectra. In this case the data were recorded on warming (from 80 K), with an excitation energy of 380 nm, after annealing at 446 K followed by slow cooling. With this thermal history the PF2/6 sample will adopt the well-ordered hexagonal phase structure. The qualitative behavior of the full FC intensity profile is very similar to that of the unannealed or lower temperature annealed PF2/6 except for a slow monotonic loss in overall intensity after the repeated stepwise thermal cycling to increasingly higher temperatures. This may indicate ongoing chemical or physical degradation during formation of the ordered hexagonal phase and mediates an increase in nonluminescent exciton decay pathways. We will revisit this last point later in the paper.

There is, as expected, significant self-absorption, and so the first emission feature fully resolved is the 0−1 FC vibronic band. The tail of the 0−0 band, which incorporates 0−n vibronic replicas from low-energy torsional modes,[53] is visible at 80 K, and this suggests either a sharpening of the absorption edge or, more likely, an increase in relative emission of excitons from states of lower energy. Perhaps most significant is the singular absence of dramatic change in the spectroscopic properties either during thermal cycling or after formation of the well-ordered hexagonal phase. Warming from 80 K produced a monotonic drop in PL intensities with no clear-cut indications of a thermochromic phase transition. Even at temperatures that span the transition to the LCP phase, and include the aforementioned abrupt change in the chain axis repeat, there are only smooth variations.

Systematic changes occur in the position of the FC vibronic bands. A 4 nm blue shift is seen on heating from 80 K to rt. Thermal annealing/cycling at elevated temperatures produces an irreversible 2−3 nm (∼20 meV) red shift as depicted in Figure 4, inset. This characteristic already occurred after heating to only 353 K (see the point labeled 1) and so must be correlated with the glass transition. This shift may indicate changes in the average PF2/6 chain conformation or, alternatively, be directly related to small but irreversible changes in the mass density.[53]

Most peculiar is a marked and persistent *red* shift of the vibronic bands on heating above 260 K. A portion of this red shift is clearly caused by the process of thermal annealing, but this attribute is retained even after heating to 470 K (well above the LCP transition temperature). This shift is counter to the commonly accepted notion that warming is associated with increasing chain conformational disorder (or a reduced density) and thereby an overall blue shift in the spectral absorption/emission bands. The blue-most position of the 0−1 vibronic band maximum occurs near 260 K, and this temperature is also below those at which the peaks in the X-ray data, from either equatorial or nonequatorial reflections, are most pronounced and sharpest. There is some possibility that the anomalous red shift is artifactual and results from either increased long wavelength self-absorption at higher temperatures or variations in the relative intensities in the subbands comprising the 0−1 band. The former effect will not alter the 0−2 band, and the absence of a continuing red shift is qualitatively reflected in this vibronic band as well. Heterogeneity at molecular length scales is yet another possibility. If, for example, the emission is comprised of two distinct classes of chromophores, then the relative contributions may be temperature dependent. We also mention that anomalous thermochromism has also been observed in helical poly(dialkylsilane) polymers,[54] and so there may be something special about helical conformations. All told, there are only subtle correlations between the bulk structural phase behavior and the optical emission line shapes.

Example PL data are shown in Figure 5 in a site-selective fluorescence[55,56] (SSF) format (in which chromophores in resonance are selectively excited) at excitation energies that sweep through the so-called exciton mobility edge. This is inferred in these spectra as a threshold energy at which the F−C emission becomes

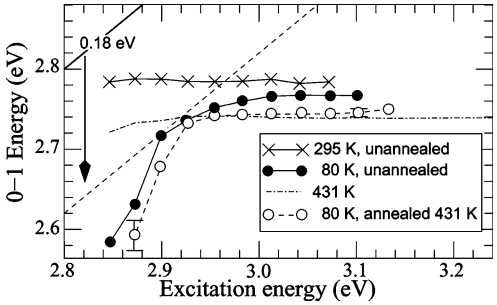

Figure 6. Plot of 0−1 vibronic band center vs excitation energy for various indicated temperatures and conditions. The 0.18 eV dotted line represents the expected energy difference between the 0−0 and 0−1 emissions bands (halfway between 160 and 200 meV, the two model specified vibronic subbands).

excitation energy dependent. All data were fit under the assumption that 0−1 band represents a superposition of two Gaussian subbands, separated by 40 meV, superimposed on a linear background. Room temperature spectra show little or no site selectiveness, presumably because both energy migration and transfer are thermally assisted processes. At reduced temperatures there is local trapping of excitons, and for bulk PF2/6 at 80 K, we observe an apparent 0−1 mobility edge of ~450 nm (2.73 or 2.91 eV in reference to the 0−0 band), in general agreement with earlier results of Bauer[57] and Meskers.[55,58] At this point a subset of the excitons can no longer migrate to lower energy chain conformational sites, and so, assuming a one-to-one response, the emission will directly track the excitation energy. The onset of SSF can also be seen by plotting the excitation energy or, more appropriately, this energy minus the nominal 180 meV offset of the 0−1 FC band against average 0−1 vibronic band position, and these data are shown in Figure 6. The one-to-one correlation may be marginally true at the onset (of the SSF), but at the lowest excitation energies there are pronounced shifts in the exciton emission in excess of that of the excitation line shift. Similar results have been seen in a few substituted poly(*p*-phenylenevinylenes) in earlier SSF studies.[59] Although the underlying explanation for this behavior is unknown, we can suggest a possible origin. In optically dense films the penetration depth will be very sensitive to excitation wavelength at the absorption edge and thus the lower energies will probe a far larger volume of material. In this way very dilute sites can be excited and detected. Quantitative analysis of the self-absorption is necessary to validate this scenario.

Another result is the observation of a broad residual low-energy emission at excitation energies well below those capable of producing FC-type emission. This response is shown in terms of PL and PLE curves in Figure 7 at 80 and 431 K. We attribute this emission primarily to the presence of chemical defects. In the SSF spectra at 80 K we observe two distinct peaks centered 515 and 550 nm. This characteristic is apparent in other PF2/6 data[60] but is not well resolved at rt.[49] In the Romaner paper[60] this low-energy emission is strongly enhanced by incorporating a large percentage of fluorenone sites. Because the overall spectral response of these two features is seen to be relatively insensitive to excitation energies ranging from 3.10 to 2.48 eV (400 to 500 nm, respectively), they conclude that the lower energy peak is likely vibronic in origin. In our case, in which the defect concentration is much lower, the emission intensity, position, and, to a lesser extent, line

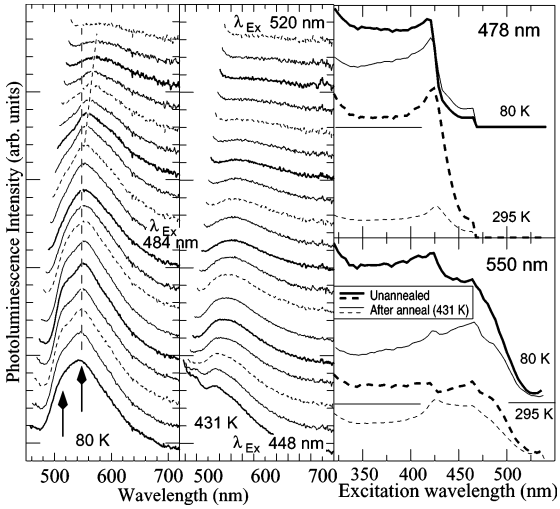

Figure 7. PL spectra at 80 K (left) and at 431 K (center) of the long wavelength defect emission as the excitation wavelength is swept from 448 to 520 nm in 4 nm steps. Bold arrows identify the appearance of two emission peaks, and the dashed lines identify the onset of energy dependent shift in the position of the 550 nm feature. All spectra are offset and scaled slightly for clarity. On the right are various PLE spectra recorded at 478 nm (top) and at 550 nm (bottom).

shape are all sensitive to temperature and excitation energy. There is also a shift of the low-energy emission feature with an onset at a 484 nm excitation wavelength. In this case the evidence is more consistent with a hypothesis of two emitting species.

Because this sample is optically dense, the PLE spectra should qualitatively resemble the absorption spectra. All 550 nm excitation spectra generally show a gradual intensity rise with an onset of 525 nm and then two additional features appearing at approximately 470 and 420 nm. The initial rise at 525 nm is likely correlated with direct excitation of the defect emission at 550 nm while the 470 nm edge will similarly correspond to the 515 nm feature. It again seems unlikely that the 550 nm peak in the SSF curves is a vibronic replica because of the rather low-energy onset (i.e., at 525 nm) in the 550 nm PLE data. The excitation peak near 420 nm is most clearly resolved in the 478 nm excitation spectra with an ill-defined onset ranging from 430 to 450 nm. A portion of this emission may be correlated with the high-energy side of 515 nm PL peak. This 430−450 nm range occurs where one expects the excitation line to first sweep through the 0−0 $\pi-\pi^*$ absorption edge. The 420 nm peak is only a minor constituent in the 550 nm excitation spectra. At 550 nm there is still appreciable intrachain FC emission (at the position of the 0−4 FC band), and so all interchain excitations that originate from direct $\pi-\pi^*$ excitations, if present at all, must be very weak. This is consistent with prior observations by List and co-workers.[47,60]

Finally, we note the significant reduction in overall emission intensity as the PF2/6 is repeatedly cycled to increasingly higher temperatures. All postanneal excitation spectra are lower in intensity, and the effect is most pronounced in the 478 nm excitation curve at 295 K. In some instances thermal annealing has been used to improve light-emitting diode efficiencies.[61] For PF2/6 it appears that evolution toward the ordered helical phase significantly increases in the presence of quenching sites. The microscopic nature of these sites cannot be explicitly identified.

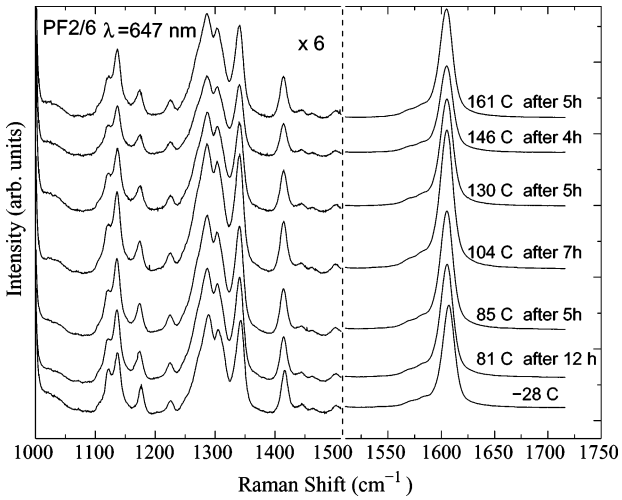

Figure 8. Selected Raman scattering spectra spanning the region from 1100 to 1750 wavenumbers. The region under 1500 cm^{-1} has been magnified a factor of 6. All spectra are offset for clarity.

C. Raman Scattering. Raman scattering probes structure at a more local level and this too has been the subject of previous PF2/6 studies.[36] The overall insensitivity of the electronic $\pi-\pi^*$ optical properties to the temperature-dependent structural phase behavior may also imply that Raman-active vibrational modes relating to the skeletal fluorene units are relatively fixed. The Raman spectra were measured from bulk PF2/6 as a function of temperature with similar time/temperature scales as in the X-ray data.

Figure 8 displays typical spectra in the range 1000−1700 cm^{-1} during the first thermal cycle (with the vertical scale expanded by 6 × at 1500 cm^{-1} and below). Raman frequencies in the 1100−1200 cm^{-1} region are most sensitive to side group substitution. The two peaks at 1120 and 1137 cm^{-1} in PF2/6 arise from the C−H bending modes of the 2-ethylhexyl side group. PFs with nonbranched side groups such as PF6 and PF8 show a single peak[62] at ∼1135 cm^{-1}, although crystalline PF8 shows a shoulder peak at 1118 cm^{-1}.[38] The 1170 and 1220 cm^{-1} peaks likely correspond to C−H bending modes from the backbone. The entire 1250−1350 cm^{-1} region shows subtle differences among the various reported PF derivatives. The 1290, 1308, and 1342 cm^{-1} peaks are associated with the backbone C−C stretch modes. The higher frequency peak at 1342 cm^{-1} is most likely the C−C stretch mode from within the more rigid monomer unit since the C−C stretch frequencies between adjacent monomer units are expected to have a lower frequency due to the allowed torsional degree of freedom. In a fluorene molecule the 1300 cm^{-1} peak has been assigned to the $C_{4a}C_{4b}$ stretching mode within the monomeric unit.[63] In polyfluorene the frequency of this mode would be expected to increase due to the enhanced stiffness of the C−C bond.

The Raman peaks in the 1600 cm^{-1} region arise from the intra-ring C−C stretch mode. This region is best fit with two peaks: a weak peak at 1582 cm^{-1} and a strong peak at 1605 cm^{-1}. There are a number of infrared (IR) peaks in the 1000−1500 cm^{-1} range with the strongest IR peak being at 1500 cm^{-1}.[24] The weak 1500 cm^{-1} band observed in the Raman spectra is most likely an activated IR peak due to a lowering of symmetry.[64]

Upon thermal cycling the changes in the Raman spectrum are more subtle compared to the changes seen in XRD. These changes occur mainly in terms of the peak positions and relative intensities. These data were fit assuming Lorentzian line shapes to determine the peak positions. Figure 9 shows the positions of the 1175, 1342, 1417, and 1605 cm^{-1} Raman peaks as a function of temperature. The filled triangles are the peak positions upon increasing the temperature while the inverted triangles represent the cooling cycle. All the Raman peaks (even those that are not plotted in the figure) exhibit similar trends upon thermal cycling although the exact magnitudes of the shifts vary somewhat. These data can be understood on the basis of the XRD data. Between 80 and 150 °C, the peak positions remain almost unchanged, suggesting a gradual onset of the cold crystallization process. From the X-ray data we know that upon cooling the hexagonal phase shows enhanced packing and improved long-range order; this is reflected in the Raman data as well. The Raman frequencies shift upward almost linearly upon cooling. This effect is associated with the decrease in the intermolecular distance due to the contraction of the ordered phase upon cooling, leading to an increase in the intermolecular and intramolecular quasi-elastic constants of the ordered state.[65]

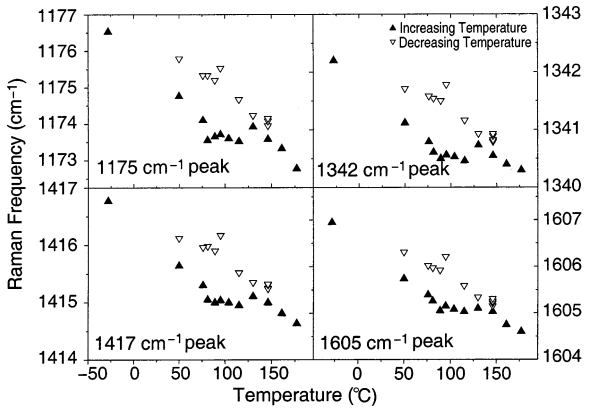

Figure 9. Peak positions of the 1175, 1342, 1417, and 1605 cm^{-1} Raman frequencies as a function of thermal cycling. The filled triangles denote the peak positions during the heating cycle, and the inverted open triangle represent the peak positions upon cooling. Between T_g and the LCP transition the Raman peak positions remain almost unchanged.

Liem et al.[62] have measured the temperature-dependent shift of the 1605 cm^{-1} Raman peak in PF8 and PF6. The shift of the 1605 cm^{-1} in PF6 is linear upon heating and cooling. PF8, on the other hand, shows a distinct discontinuity at 150 °C. Between 50 and 150 °C the frequency of the 1605 cm^{-1} peak remains fairly constant in PF8, similar to what we see in PF2/6. Presumably this is dependent on the local chain conformation and packing which is very sensitive to the explicit side chain moiety in tandem with the main chain conformation. Thus, there should be parallels between PF8 and PF2/6 in this regard even though the explicit conformations remain unknown.

The peak intensities of the C−H bend modes originating from the alkyl side chain display an unexpected anomaly at low temperature. Figure 10 shows the relative intensity ratios of the 1120 cm^{-1} to 1137 cm^{-1} (I_{1120}/I_{1137}) and the 1175 cm^{-1} to the 1137 cm^{-1} (I_{1175}/I_{1137}) Raman peaks. Between 11 and 40 K the I_{1120}/I_{1137} ratio rapidly changes from ∼1 to 0.7, beyond which there is a linear decrease in the intensity ratio until T_g. The I_{1175}/I_{1137} ratio, on the other hand, shows a linear decrease in intensity without any significant disconti-

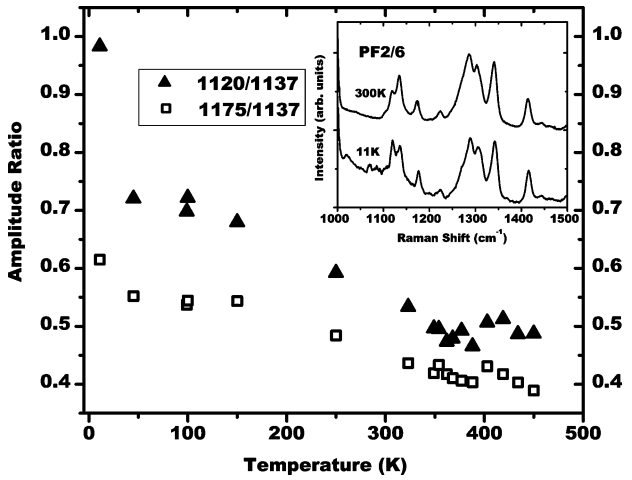

Figure 10. Relative intensity ratios of the 1120−1137 cm^{-1} (filled triangles) and the 1175−1137 cm^{-1}(open squares) Raman peaks. The inset shows the Raman spectrum of bulk PF2/6 at 11 and 300 K.

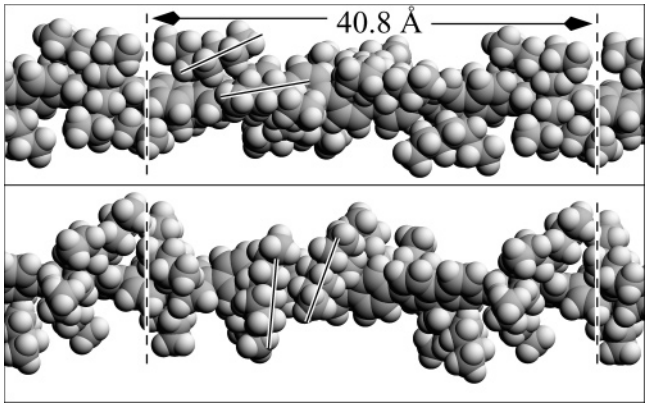

Figure 11. Top: side view of starting 5/2 helix model (with core side chain dihedral angles of a_0g+g+/a_0g+g+). The solid lines indicate pairing of the side chains and an orientation along the helical axis. Bottom: side view of final chain structure resulting from the structure factor refinement. The solid lines indicate pairing of the side chains and an orientation more perpendicular to the chain axis.

nuities at low temperatures. The sharp drop in intensity of the 1120 cm^{-1} peak between 11 and 40 K cannot be attributed to any gross structural change. There may be a temperature-sensitive coupling of the low-energy torsion modes with the 1120 cm^{-1} frequency.

D. Modeling and Structure Factor Refinement. Molecular level modeling of PF2/6 is difficult because of the necessity of incorporating the 5-fold symmetry of the single chain helices into a nested three chain unit cell with, on average, hexagonal symmetry. Analysis is further complicated by the secondary constraint of interdigitating the alkyl sides from neighboring chains into a physically self-consistent three-dimensional (3D) packing. Knaapila et al. have succeeded using a single three chain aggregate, but the average interchain distances are too large to build up a composite repeating 3D structure having the experimentally determined PF2/6 lattice constants.[22]

As a prelude to the structure factor (SF) refinements, we first modeled single chain oligomers with the goal of identifying compact structures consistent with a 5/2 helix repeat. The bulky 2-ethyl side branch presents yet a third complicating issue, and so only di-*n*-hexylfluorene based oligomers were considered at first. Various side chain conformations were specified assuming either gauche (g+), gauche′, (g−), or anti (a_0) C−C dihedral angles. A single *n*-hexyl side chain would require one to specify five torsion angles. In the discussion that follows we refer only to the three core C−C dihedral angles, starting from the carbon bridge atom and moving outward. The latter two were always set to anti conformations.

One model, specifically that of a repeating array of monomers incorporating an anti-gauche−gauche (or 5/2 a_0g+g+) sequencing of the $\tau_1\tau_2\tau_3$ torsion angles (see Figure 1), provided an especially close-packed conformation, and this model is shown in Figure 11 in terms of an enantiomeric RR-PF2/6 chain. This conformer forms a locally stable zero-temperature gas-phase structure with a backbone torsion angles approximating 145°, a value close to that required for a 5/2 helix. The side chains are nested pairwise and are oriented nearly parallel to the helical axis. This was one conformation that could be readily packed into a viable 3D model and thus provided a starting point for the refined structure that follows. To obtain the PF2/6 moiety, we added, ad hoc, the 2-ethyl branches, assuming just a single RR-type enantiomer.

Initial fits to the data were poor because of the widespread occurrence of large scattering intensities at Bragg reflections not seen in the data (most notably with l = 2, 3, and 4). Maximizing the intensity of the experimentally resolved nonequatorial scattering peaks proved difficult. In particular, there was little intensity within the l = 5 layer line when the alkyl side chains are oriented nearly parallel to the main chain axis. Iterative refinements that alternatively allowed for increased side chain motion and increased weighting of the hard-core packing constraints in combination with all other allowed degrees of freedom greatly improved the fit to the experimental data (this model is included in the Supporting Information). Figure 12 displays the best fit to the hexagonal phase data at 115 °C (on cooling). At this temperature, the Bragg peaks are sharp and the (005) reflection is segregated from the various reflections comprising the (110) peak. Although clearly imperfect, the calculated profile generally reproduces most of the major systematic intensity variations in the data. In particular, this model can achieve strong l = 1 and l = 5 layer line intensities.

The best-fit unit cell parameters are marginally monoclinic (a = 17.1 Å, b = 17.0 Å, c = 40.8 Å, γ = 120.4°, ρ = 0.94 g/cm^3). These are very close to hexagonal and comparable to values reported previously.[17,34] Knaapila and co-workers[22] report a much more distorted unit cell geometry in PF2/6 ultrathin films. The key model specific attributes necessary for a strong (005) reflection are (1) all three chains comprising the unit cell axially in-phase (as much as possible) with respect to the nominal 8 Å monomer repeat and (2) the side chains oriented near normal to the skeletal backbone. The strong and ever present scattering at this *d*-spacing, even in the LCP phase, indicates that a significant fraction of the alkyl side chains are always oriented perpendicularly to the *c*-axis direction. To achieve this result in a 5/2 helix and simultaneously reconcile local structure packing constraints, the alkyl side chains include one or more gauche conformers at the three C−C sites closest to the carbon bridge atom. There is also a significant proportion of pairwise packing of these alkyl side chains. The final refined chain structure can be seen in the bottom panel of Figure 11. Some combination

of the these attributes is likely to be necessary for fitting of the nonequatorial scattering data in PF6, PF8, and related polymers. Additionally, two of the three chains within a unit cell are displaced laterally in the equatorial plane from positions of high symmetry. We cannot unambiguously rule out other local molecular level structural responses. The alternative 5/1 helix cannot be eliminated from consideration either, but this helix is even more difficult to pack into the stated unit cell if the side chains are oriented normal to the *c*-axis direction. The core of a 5/2 helix is considerably more compact than that of the 5/1.[17]

The pentagonal aspect of the PF2/6 helix in combination with a multitude of alkyl side chain conformations likely frustrates crystallization of the side chains. Large-scale ordering of the side chains may actually conflict with spacings along the polymer backbone or those associated with long-range order of the unit cell. Since the XRD represents the average unit cell structure, a true resemblance to the actual molecular packing may be limited. Still we note that a large multioligomer cluster based on the SF refinement model exhibited only modest changes in the local chain structures and packing when subjected to a simple zero-temperature energy minimization using MM3 force-field parameters. The explicit chain conformation identified here is *unlikely* to be unique. However, the general attributes will be present in any other explicit configuration.

As a supplement to the SF calculations, a large number of single chain decamers were modeled by systematically varying both the backbone and side chain conformation. As already noted, a combinatorial approach has proven useful for identifying low-energy conformations in other alkyl-substituted polymers.[21,32,33] For PFs the alkyl chain spacing along the backbone is much sparser, and so interchain interactions could be expected to play a more dominant role. In view of the X-ray evidence for cold crystallization and, thereafter, the relatively few overt changes in the average PF2/6 backbone conformation on thermal cycling, this suggests that the chain conformational structure is already established while in solution, and the main impact of interchain interactions is to influence side chain order on local length scales. Thus, a single chain study may have relevance to the solid state.

Explicitly we considered all permutations (anti, gauche, gauche′) of the three core side chain dihedral angles (see Figure 1), assuming, initially, ±5/1, ±5/2, 2/1 (this with a dyad construction of alternating + then −165° fluorene−fluorene torsion angles), and all-anti repeats of the fluorene backbone. To reference a distinct side chain conformer, we employ the notation of, for example, /a_0g+t+/ to represent C−C dihedral conformers as one moves outward from the carbon bridge atom (see Figure 1). The addition of the 2-ethyl branch alters the local pairwise interaction so that conformations intermediate to gauche or anti appear.[17] The representative set includes a_0 (anti), t± (transoid), d± (deviant, from the notation of ref 66), g± (gauche), and c± (cisoid) for nominal dihedral angle magnitudes of >175°, 175° to 160°, 160° to 100°, 100° to 40° and 40° to 5°, respectively.

We note that no planar or near planar structures were obtained in the all-anti trials, and so these results are not included. Many of the starting trial structures were unphysical (due to hard-core packing constraints) and thus resulted in disordered final structures or, less frequently, evolved into regular structures of closely

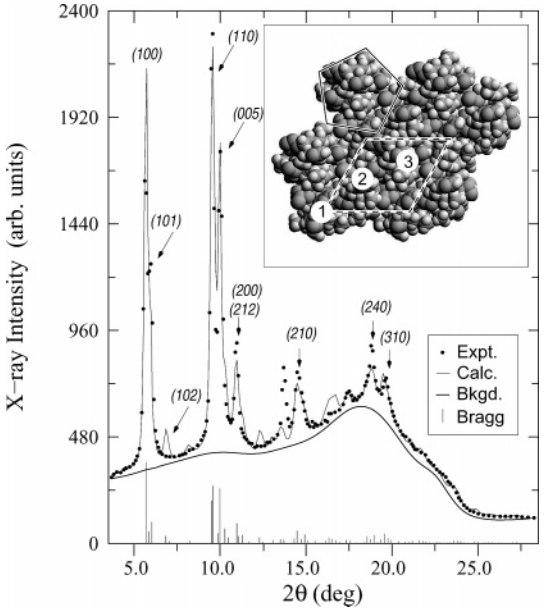

Figure 12. Comparisons of experimental (small dots) and calculated (thin line) X-ray diffraction patterns in PF2/6 at 115 °C after heating to the LCP phase. Vertical lines are a histogram of the Bragg intensities. Inset: real space equatorial projection of the unit cell containing three 5/2 helices.

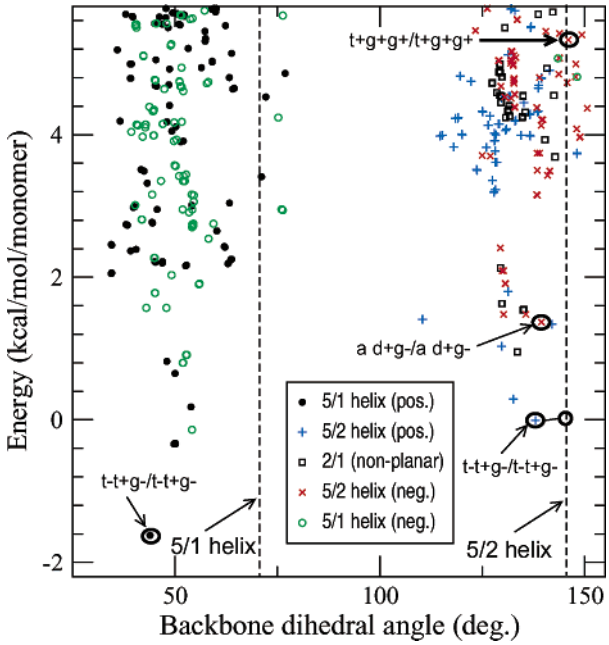

Figure 13. Results of combinatorial search for low-energy PF2/6 conformers using MM3* force-field parameters under the assumption of a single repeating monomer conformation. Each symbol corresponds to a single, unique conformer, and the bold arrow points to the 5/2(−) t+g+g+ /t+ g+ g+ starting conformer used in the structure factor calculations (Figure 11, top). All energies are referenced to the lowest energy conformer having a positive constrained 5/2 helix and two t−t+g− type side chains. The one identified in the figure is not torsionally constrained. See text for more details.

related conformations. Both these have been excluded from the relevant figures and further discussion. Figure 13 plots all "stable"[67] RR-type PF2/6 conformers with energies less than ~6 kcal/mol/monomer when normalized to the lowest energy 5/2 helix conformer identified (a positive 5/2 helix with two t−t+g− type side chains and constrained to a 5/2 helix). The reference conformer is indicated by the open circle at zero energy. The

sensitivity to changes in the torsion angle setting is quite small, and in the absence of interchain interactions, a high degree of polyfluorene conformational disorder is likely. These data actually represent a fairly small subset of the 4000+ starting conformations tested. A more exhaustive study would require similar tests of the SR- and RS-type PF2/6 conformers in addition to examining dyads and more complicated repeating structures. This is beyond the scope of the present work.

Most apparent in Figure 13 is the modest numbers of viable low-energy conformers compatible with the nominal 5/1, 5/2, and/or 2/1 type backbone conformations. In the absence of interchain interactions, solvent effects, or any other secondary packing constraints there is little obvious preference for any one particular structure. Hence, the chain conformational disorder will be substantial unless there are additional ordering mechanisms. The overall distribution has a number of interesting properties. All starting backbone conformations generally give rise to monomodal distributions. One nominal helix conformer, i.e., t−t+g−/t−t+g−, is especially low in energy for just positive helicity chains and, if it is in any way dominant in the real material, then could predispose PF2/6 to helical phases. Leiser et al.[17] identify this side chain conformer in monomer studies. Surprisingly this conformational isomer is lowest in energy in the case of a "5/1" helix, but the backbone dihedral angle of approximately 43°, if correct, is clearly incompatible with a 5/1 helical repeat. On average the 5/2 type conformational isomers have torsion angles closer to the ideal case of ∼145°.

Figure 13 also demonstrates that the a_0g+g+/a_0g+g+ conformer used to initiate the SF refinement (identified as t+g+g+/t+g+g+) is simply one of many representative of lower energy conformers. Although this conformation can be considered a reasonable starting point, it is not surprising that the resulting best-fit SF chain structure is much different than that at the start. The refined SF model has side chains that retain some fraction of gauche isomers. At this point a one-to-one mapping between this modeling and the X-ray analysis is still not possible because the pairwise alkyl packing seen in the SF calculations requires, at a minimum, a more exhaustive search that includes asymmetric 2-fold pairings of the alkyl side chains.

IV. Conclusions

Despite striking changes in long-range order in PF2/6 on thermal cycling, the observed impact on the resulting PF backbone conformation and that of the photophysics are limited and subtle. The only exception is the loss in emission intensity. This is very different than the situation for two closely related PF derivatives, PF6 and PF8, in which both intrachain and interchain photoexcitations are strongly altered. Modeling indicates a large but limited number of low-energy conformers that, on average, yield a monomodal distribution of backbone torsion angles and some indication of a preference for helices. Before definitive conclusions are drawn, the efficacy of this approach needs to be further tested and more complex conformational sequences similarly examined.

Structure factor calculations are consistent with the presence of 5/2 helices but cannot explicitly rule out all other 5-fold helical conformations. The large-scale ordering that PF2/6 undergoes in response to thermal cycling probably alters the explicit set of representative conformers, but these are drawn from the same aforementioned monomodal distribution. Thus, the optical properties are little changed. We expect that the development of long-range order involves major changes in the conformation and packing of the alkyl side chains. Large-scale crystallization of the side chains does not appear. Further elucidation of this process requires better structural probes of the alkyl side chains [e.g., NMR, IR and/or Raman (beyond 2000 cm^{-1}) spectroscopy].

SF calculations are indicative of a strong tendency to order alkyl side chains in a pairwise fashion along the helix. These side chains are pointed, more or less, normal to the helical axis, and the polyfluorene core is physically occluded. This strongly suppresses formation of any close interchain contacts and limits the extent of interchain excitations. Thus, the resulting photophysics is dominated by exciton emission and, if broad low-energy PL is present, that of chemical defects. PLE spectroscopy clearly identifies two emitting chromophores. Even in a "ordered" form PF2/6 incorporates a large number of conformational isomers. Thus, it is best referred to as a conformationally disordered (i.e., condis) crystal.[68] Overall, the structure models presented here may have sufficient merit for use as starting points in quantum chemical calculations that address the role of intrachain disorder in the resulting photophysics.

A long-standing question that still remains unanswered is how eliminating the 2-ethyl branch explicitly alters the intrachain and interchain packing in the *n*-alkyl polyfluorenes. There are some direct indications of interchain close packing in PF6[21] and other PF derivatives,[23] but these models remain speculative. The well-spaced PF8 chain packing in the recent report by Chen[20] has merit, but the model as whole is still tentative. Additional studies and analysis are needed for a more comprehensive understanding of the molecular structure.

Acknowledgment. We gratefully acknowledge the support of this work through NSF Grants DMR-0350383 (B.T. and M.J.W.). S.G. acknowledges the donors of the American Chemical Society Petroleum Research Fund (No. 38193-B7) for partial support of this work. S.G. thanks M. Chandrasekhar for access and use of her research laboratory and useful discussions. M.J.W. thanks M. Knaapila for access to prior modeling results and M. Knaapila, J. Gierschner, and L. Rothberg for useful discussions and comments.

Supporting Information Available: MM3* energies of various conformers. This material is available free of charge via the Internet at http://pubs.acs.org.

References and Notes

(1) Scherf, U.; List, E. J. W. *Adv. Mater.* **2002**, *14*, 477.
(2) Neher, D. *Macromol. Rapid Commun.* **2001**, *22*, 1366.
(3) Leclerc, M. *J. Polym. Sci., Part A* **2001**, *39*, 2867.
(4) Tirapattur, S.; Belletete, M.; Drolet, N.; Bouchard, J.; Ranger, M.; Leclerc, M.; Durocher, G. *J. Phys. Chem. B* **2002**, *106*, 8959.
(5) Geng, Y. H.; Culligan, S. W.; Trajkovska, A.; Wallace, J. U.; Chen, S. H. *Chem. Mater.* **2003**, *15*, 542.
(6) Nakazawa, Y. K.; Carter, S. A.; Nothofer, H. G.; Scherf, U.; Lee, V. Y.; Miller, R. D.; Scott, J. C. *Appl. Phys. Lett.* **2002**, *80*, 3832.
(7) Grell, M.; Bradley, D. D. C.; Ungar, G.; Hill, J.; Whitehead, K. S. *Macromolecules* **1999**, *32*, 5810.
(8) Li, Y. N.; Vamvounis, G.; Holdcroft, S. *Macromolecules* **2002**, *35*, 6900.

(9) Winokur, M. J.; Spiegel, D.; Kim, Y. H.; Hotta, S.; Heeger, A. J. *Synth. Met.* **1989**, *28*, C419.
(10) Grell, M.; Bradley, D. D. C.; Inbasekaran, M.; Ungar, G.; Whitehead, K. S.; Woo, E. P. *Synth. Met.* **2000**, *111*, 579.
(11) Redecker, M.; Bradley, D. D. C.; Inbasekaran, M.; Woo, E. P. *Appl. Phys. Lett.* **1999**, *74*, 1400.
(12) Oda, M.; Nothofer, H. G.; Scherf, U.; Sunjic, V.; Richter, D.; Regenstein, W.; Neher, D. *Macromolecules* **2002**, *35*, 6792.
(13) Geng, Y. H.; Trajkovska, A.; Katsis, D.; Ou, J. J.; Culligan, S. W.; Chen, S. H. *J. Am. Chem. Soc.* **2002**, *124*, 8337.
(14) Cadby, A. J.; Lane, P. A.; Mellor, H.; Martin, S. J.; Grell, M.; Giebeler, C.; Bradley, D. D. C.; Wohlgenannt, M.; An, C.; Vardeny, Z. V. *Phys. Rev. B* **2000**, *62*, 15604.
(15) Winokur, M. J.; Slinker, J.; Huber, D. L. *Phys. Rev. B* **2003**, *67*, 4106.
(16) Cheun, H.; Tanto, B.; Chunwachirasiri, W.; Larson, B.; Winokur, M. J. *Appl. Phys. Lett.* **2004**, *84*, 22.
(17) Lieser, G.; Oda, M.; Miteva, T.; Meisel, A.; Nothofer, H. G.; Scherf, U. *Macromolecules* **2000**, *33*, 4490.
(18) Leclere, P.; Hennebicq, E.; Calderone, A.; Brocorens, P.; Grimsdale, A. C.; Mullen, K.; Brédas, J. L.; Lazzaroni, R. J. *Prog. Polym. Sci.* **2002**, *28*, 55.
(19) Leclerc, M.; Ranger, M.; Belanger-Gariepy, F. *Acta Crystallogr. C* **1998**, *54*, 799.
(20) Chen, S. H.; Chou, H. L.; Su, A. C.; Chen, S. *Macromolecules* **2004**, *37*, 6833.
(21) Winokur, M. J.; Chunwachirasiri, W. *J. Polym. Sci.* **2003**, *41*, 2630.
(22) Knaapila, M.; Lyons, B. P.; Kisko, K.; Foreman, J. P.; Vainio, U.; Mihaylova, M.; Seeck, O.; Pålsson, L.; Serimaa, R.; Torkkeli, M.; Monkmann, A. P. *J. Phys. Chem. B* **2003**, *107*, 12425.
(23) Surin, M.; Hennebicq, E.; Ego, C.; Marsitzky, D.; Grimsdale, A. C.; Mullen, K.; Brédas, J. L.; Lazzaroni, R.; Leclere, P. *Chem. Mater.* **2004**, *16*, 994.
(24) List, E. J. W.; Guentner, R.; de Freitas, P. S.; Scherf, U. *Adv. Mater.* **2002**, *14*, 374.
(25) Prosa, T. Ph.D. Thesis, University of Wisconsin, 1996.
(26) Prosa, T. J.; Winokur, M. J.; Moulton, J.; Smith, P.; Heeger, A. J. *Macromolecules* **1992**, *25*, 4364.
(27) Duparcmeur, Y. L.; Gervois, A.; Troadec, J. P. *J. Phys. C: Condens. Matter* **1995**, *7*, 3421.
(28) Nishimura, H.; Sarko, A. *Macromolecules* **1991**, *24*, 771.
(29) A standard MM3 force field with minor modifications to account for conjugation in the molecular modeling package, MacroModel, Schrodinger Inc. (see http://www.schrodinger.com). The MM3 program itself is available to all users from Tripos Associates, 1699 South Hanley Road, St. Louis, MO 63144.
(30) Rasmol, a molecular viewer, is freely available at http://www.rasmol.org/.
(31) Convergence was assumed when the energy minimization gradient dropped below 0.02 kJ/mol (for the decamer). A maximum of 15 000 minimization steps were allowed.
(32) Winokur, M. J.; West, R. *Macromolecules* **2003**, *36*, 7338.
(33) He, Z.; Prud'homme, R. E. *Macromolecules* **1999**, *32*, 7655.
(34) Kawana, S.; Durrell, M.; Lu, J.; Macdonald, J. E.; Grell, M.; Bradley, D. D. C.; Jukes, P. C.; Jones, R. A. L.; Bennett, S. L. *Polymer* **2002**, *43*, 1907.
(35) Knaapila, M.; et al., preprint.
(36) Bradley, D. D. C.; Liem, H., private communication.
(37) Nothofer, H.-G. Ph.D. Thesis, University of Potsdam, 2001.
(38) Ariu, M.; Lidzey, D. G.; Bradley, D. D. C. *Synth. Met.* **2000**, *111*, 607.
(39) Papadopoulos, P.; Floudas, G.; Chi, C.; Wegner, G. *J. Chem. Phys.* **2004**, *120*, 2368.
(40) Hosemann, R.; Bagchi, S. N. *Direct Analysis of Diffraction by Matter*; North-Holland: Amsterdam, 1962.
(41) Prosa, T. J.; Moulton, J.; Heeger, A. J.; Winokur, M. J. *Macromolecules* **1999**, *32*, 4000.
(42) Rothe, C.; Guentner, R.; Scherf, U.; Monkman, A. P. *J. Chem. Phys.* **2001**, *115*, 9557.
(43) Rothe, C.; Hintschich, S. I.; Palsson, L. O.; Monkman, A. P.; Guentner, R.; Scherf, U. *Chem. Phys. Lett.* **2002**, 360, 111.
(44) Dias, F. B.; Macanita, A. L.; de Melo, J. S.; Burrows, H. D.; Guntner, R.; Scherf, U.; Monkman, A. P. *J. Chem. Phys.* **2003**, *118*, 7119.
(45) Guha, S.; Rice, J. D.; Yau, Y. T.; Martin, C. M.; Chandrasekhar, M.; Chandrasekhar, H. R.; Guentner, R.; de Freitas, P. S.; Scherf, U. *Phys. Rev. B* **2003**, *67*, 125204.
(46) Lee, J.-I.; Zyung, T.; Miller, R. D.; Kim, Y. H.; Jeoung, S. C.; Kim, D. *J. Mater. Chem.* **2000**, *10*, 1547.
(47) Zojer, E.; Pogantsch, A.; Hennebicq, E.; Beljonne, D.; Brédas, J. L.; de Freitas, P. S.; Scherf, U.; List, E. J. W. *J. Chem. Phys.* **2002**, *117*, 6794.
(48) Lupton, J. M.; Craig, M. R.; Meijer, E. W. *Appl. Phys. Lett.* **2002**, *80*, 4489.
(49) Hintschich, S. I.; Rothe, C.; Sinha, S.; Monkman, A. P.; de Freitas, P. S.; Scherf, U. *J. Chem. Phys.* **2003**, *119*, 12017.
(50) Rothberg, L., private communication.
(51) Bliznyuk, V. N.; Carter, S. A.; Scott, J. C.; Klärner, G.; Miller, R. D.; Miller, D. C. *Macromolecules* **1999**, *32*, 361.
(52) Herz, L. M.; Silva, C.; Phillips, R. T.; Setayesh, S.; Mullen, K. *Chem. Phys. Lett.* **2001**, *347*, 318.
(53) Gierschner, J.; Mack, H. G.; Luer, L.; Oelkrug, D. *J. Chem. Phys.* **2002**, *116*, 8596.
(54) Schilling, F. C.; Lovinger, A. J.; Zeigler, J. M.; Davis, D. D.; Bovey, F. A. *Macromolecules* **1989**, *22*, 3055.
(55) Meskers, S. C. J.; Hubner, J.; Oestreich, M.; Bässler, H. *Chem. Phys. Lett.* **2001**, *339*, 223.
(56) Bässler, H.; Schwitzer, B. *Acc. Chem. Res.* **1999**, *32*, 173.
(57) Bauer, C.; Urbasch, G.; Giessen, H.; Meisel, A.; Nothofer, H. G.; Neher, D.; Scherf, U.; Mahrt, R. F. *Chem. Phys. Chem.* **2000**, *1*, 142.
(58) Meskers, S. C. J.; Hübner, J.; Oestreich, M.; Bässler, H. *J. Phys. Chem. B* **2001**, *105*, 9139.
(59) Harrison, N. T.; Baigent, D. R.; Samuel, I. D. W.; Friend, R. H.; Grimsdale, A. C.; Moratti, S. C.; Holmes, A. B. *Phys. Rev. B* **1996**, *53*, 15815.
(60) Romaner, L.; Pogantsch, A.; de Freitas, P. S.; Scherf, U.; Gaal, M.; E. Z.; List, E. J. W. *Adv. Funct. Mater.* **2003**, *13*, 597.
(61) Niu, Y. H.; Hou, Q.; Cao, Y. *Appl. Phys. Lett.* **2002**, *81*, 634.
(62) Liem, H.; Etchegoin, P.; Whitehead, K. S.; Bradley, D. D. C. *J. Appl. Phys.* **2002**, *92*, 1154.
(63) Negri, F.; Zgierski, M. Z. *J. Chem. Phys.* **1992**, *97*, 7124.
(64) Martin, C. M.; Guha, S.; Chandrasekhar, M.; Chandrasekhar, H. R.; Guentner, R.; de Freitas, P. S.; Scherf, U. *Phys. Rev. B* **2003**, *68*, 115203.
(65) Sushchinskii, M. M. *Raman Spectra of Molecules and Crystals;* Keter Inc.: New York, 1994; Vol. 116, p 283.
(66) Michl, J.; West, R. *Acc. Chem. Res.* **2000**, *33*, 821.
(67) Stability is subjectively specified and implies that the resulting oligomer consisted of a single repeating conformer construction.
(68) Wunderlich, B.; Moller, M.; Grebowicz, J.; Baur, H. *Adv. Polym. Sci.* **1988**, *87*, 1.

MA049006P